Vacuum Rabi Splitting and Strong-Coupling Dynamics for Surface-Plasmon Polaritons and Rhodamine 6G Molecules

T. K. Hakala,[1] J. J. Toppari,[1] A. Kuzyk,[1,2] M. Pettersson,[3] H. Tikkanen,[3] H. Kunttu,[3] and P. Törmä[2,*]

[1]*Nanoscience Center, Department of Physics, P.O. Box 35, FI-40014, University of Jyväskylä, Finland*
[2]*Department of Applied Physics, P.O. Box 5100, FI-02015, Helsinki University of Technology, Finland*
[3]*Nanoscience Center, Department of Chemistry, P.O. Box 35, FI-40014, University of Jyväskylä, Finland*
(Received 3 February 2009; published 31 July 2009)

We report on strong coupling between surface-plasmon polaritons (SPP) and Rhodamine 6G (R6G) molecules, with double vacuum Rabi splitting energies up to 230 and 110 meV. In addition, we demonstrate the emission of all three energy branches of the strongly coupled SPP-exciton hybrid system, revealing features of system dynamics that are not visible in conventional reflectometry. Finally, in analogy to tunable-Q microcavities, we show that the Rabi splitting can be controlled by adjusting the interaction time between waveguided SPPs and R6G deposited on top of the waveguide. The interaction time can be controlled with sub-fs precision by adjusting the length of the R6G area with standard lithography methods.

In the strong-coupling regime, the Fermi golden rule fails and coherent dynamics dominates. For light, strong coupling is important, e.g., in lasing and in coherent energy transfer between excitations, relevant for light-harvesting systems. Vacuum Rabi splitting (VRS) has been observed in microcavities for inorganic [1,2] and organic [3,4] semiconductors. Surface-plasmon polaritons (SPP) provide an alternative route to enhance the coupling and extend to nanoscale. Accordingly, Rabi splitting between SPP and J aggregates was demonstrated in Refs. [5–7], and was accredited with a particularly narrow absorption linewidth of J aggregates. Here we show a double VRS between SPP and R6G molecules, having considerably wider absorption linewidths, with splitting energies of 230 and 110 meV. Because of the presence of two coupled excitons, the middle branch of the dispersion thus presents SPP-induced exciton hybridization between the two excitons in R6G molecule. Further, owing to a new measurement scheme, for the first time the emission of all three energy branches of the strongly coupled system is observed, which is promising concerning light generation and can be used to probe the system dynamics, such as energy transfer between the three exciton-SPP branches. Besides using Kretschmann geometry [8,9], we study the dynamics of strong coupling by introducing a new approach where waveguided SPPs propagate through a molecular area of controllable length, in analogy with a tunable-Q cavity. Additionally, the observation of Rabi split, despite the broad absorption linewidth of R6G, suggests the usability of a wide variety of organic molecules for achieving strong coupling.

To study the strong coupling between SPPs and R6G, sandwich structured samples were fabricated, having a glass substrate, a 45 nm silver film above it, and on the top a resist layer (50 nm, Microchem SU-8 2025) with four different concentrations of R6G. To determine the absorb-

ance of the molecular films, reference samples with no silver layer were fabricated. For the SPP waveguide studies, another set of samples was fabricated (for details, see [10,11]), allowing spectral measurements in specific locations on the sample and the control of the interaction time between R6G and SPP.

Reflectometry measurements in the Kretschmann configuration were performed [see Fig. 1, detection 1 (DM1)], yielding the dispersion relation of the energy of incoupled modes as a function of the in-plane wave vector k. Another method was used for studying the dynamics and mode emission after the incoupling [see Fig. 1, detection 2, (DM2)]. In this case we employ the scattering of the strongly coupled hybrid modes into photons from scattering centers always present in practical systems (silver impurities or small corrugations). Because of the propagation of the hybrid polaritons before scattering, the scattering event is spatially and temporally separated from the
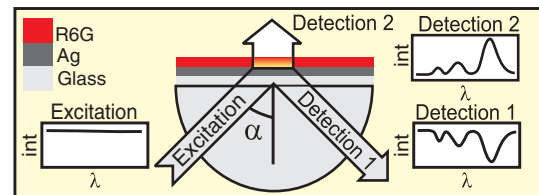

FIG. 1 (color online). The samples were studied by using three different, complementary detection methods. Detection 1 (DM1), applied before also, e.g., in Refs. [5,21,22], gives the energies that are coupled into the system as a function of in-plane wave vector k. The coupled modes are shown as dips in the reflected light. Detection 2 (DM2), not used in previous literature, gives the energies of the modes that are coupled out from the system by scattering processes. A third, waveguide-based method is introduced in Fig. 3.

incoupling. The reflected (DM1) or luminescent (DM2) light from a few-mm-sized area was collected by focusing the light into an optical fiber connected to a spectrometer. For the excitation, a collimated (<0.5 mm size), p-polarized incoherent white light source was used. The incident angle was controlled by a rotatable prism.

The dispersions measured with DM1 are shown in Fig. 2(a). For the 4 mM concentration, the dispersion has only one mode which is characteristic to a SPP on a silver–SU-8 layer–air structure, i.e., no molecular contribution. When increasing the concentration to 25 mM, an anticrossing behavior emerges at the energy corresponding to a measured absorption maximum of R6G in the SU-8 layer (2.29 eV) as a sign of the strong-coupling regime. By increasing the concentration to 50 mM, this Rabi splitting widens. When the R6G concentration is further increased to 200 mM, the existing split again widens and a second split appears at around 2.45 eV, which corresponds to a
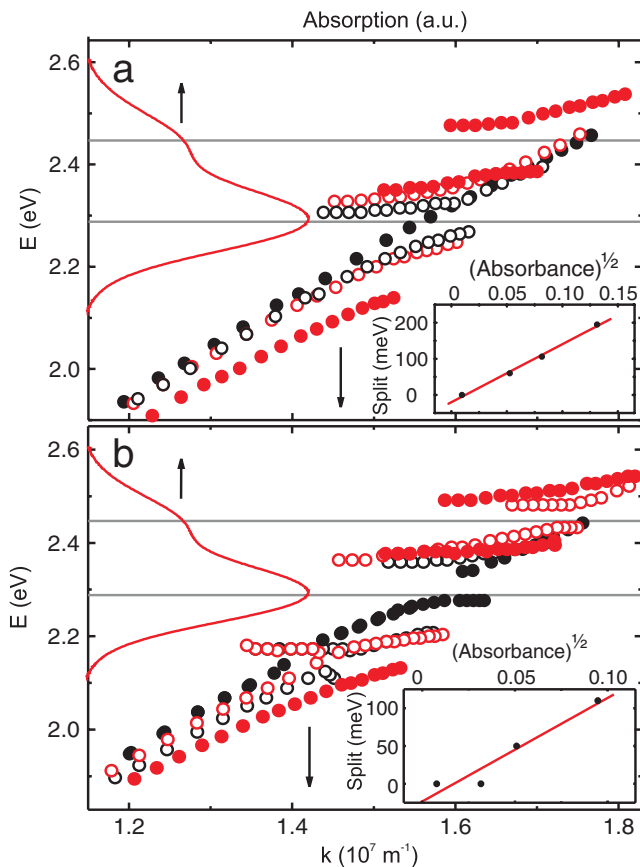
measured absorption shoulder of the R6G film. The inset of Fig. 2(a) shows the expected linear relationship between the low energy splitting and the square root of absorbance [12].

The Rabi-splitting energies for the 200 mM sample are 200 meV (main absorption) and 100 meV (absorption shoulder). The middle branch thus presents SPP-induced exciton hybridization between the two excitons. Previous observations of exciton hybridization with organic dye molecules have involved cavity photons [13,14], whereas here the SPP creates the hybridization.

Previously, the strong-coupling regime between SPPs and photoactive organic molecules has been observed only with J aggregates, with Rabi-splitting energies up to 250 meV [5–7,15–17]. For these aggregates, the Rabi splitting at room temperature has been associated with the high oscillator strength together with a small absorption linewidth [18]. It should be stressed that we observe Rabi splitting although, for each transition (the main and the shoulder), the minimum observed Rabi splitting is below the original measured widths of that transition and the uncoupled SPP. This suggests that the SPP-molecule interaction causes line narrowing as a precursor to the strong coupling [15,19,20], which was also verified by measuring the linewidths of the coupled and uncoupled modes.

To test the effect of the photon number, we varied the intensity over 2 orders of magnitude, i.e., between 0.17–13 W/m^2 over the visible range, with no effect on the splitting, consistent with VRS. Note that this is the so-called many-atom (or quantum well) VRS: many molecules are interacting coherently with the same SPP photon.

Dynamics, that is, energy transfer, propagation, and scattering, as well as dissipation mechanisms, of the hybrid modes are basic, yet scarcely studied phenomena in these systems. To study dynamics, we employ DM2 shown in Fig. 1. The spectrum measured with DM2 has negligible contribution from the reflected or transmitted excitation light: it consists of scattered hybrid SPP-exciton modes and uncoupled, spontaneous emission of R6G. Since the scattering event is temporally separated from the incoupling event, we gain insight into the dynamics of the system by comparing the energies of these two events. The excitation being the same both in DM1 and DM2 implies that all differences between the results must come from the dynamics after incoupling, not from the incoupling mechanism. Figure 2(b) shows the dispersions for the same samples, measured by DM2. We emphasize that we see emission from all three energy branches, contrary to previous reports [5,21,22], where the emission from the upper branch was always missing. In contrast to ours, the excitation in these experiments was done from the side of the molecules.

One qualitative difference between the DM1 and DM2 dispersions is that DM2 shows an additional emission branch nearly independent of the in-plane k vector at around 2.17 eV, for the 25 and 50 mM samples.

FIG. 2 (color online). The dispersions of four different samples having R6G concentrations of 4 mM (solid black circles), 25 mM (empty black circles), 50 mM (empty red or dark gray circles), and 200 mM (solid red or dark gray circles) measured by DM1 (a) and DM2 (b). The solid red or dark gray curves are the measured absorbance of the 200 mM SU-8–R6G film, and solid gray horizontal lines are the absorption maximum and absorption shoulder energies. The insets show the low (a) and high (b) energy splits as a function of (absorbance)$^{1/2}$ with linear fits.

According to the measurements of a reference sample having R6G film but no silver, this branch could be identified as the spontaneous, noncoupled, emission maximum of R6G, reported also for *J* aggregates [5,18]. The more significant difference in the dispersions is that the DM2 shows an increased energy splitting as compared to DM1, e.g., 230 and 110 meV for the 200 m*M* sample. Particularly distinctive is the difference for the 4 and 50 m*M* samples, in which the low or high energy splitting, respectively, is apparent only for DM2 [see Figs. 2(a) and 2(b) and for clearer comparison Fig. 4 with theoretical fits included].

Although the maximum VRS is proportional to $A\sqrt{N/V}$, where *A* contains the transition dipole moment, *N* is the number of oscillators and *V* the mode volume, dynamics such as decay and decoherence may decrease the Rabi splitting [23]. For instance, in case of cavities, the VRS is $2\sqrt{g^2 - (\gamma_C - \gamma_X)^2/16}$, where *g* is a coupling constant and γ_C (γ_X) is the cavity (exciton) decay rate [24,25]. The widths of the modes are given by $(\gamma_C + \gamma_X)/2$. A simple interpretation of the observed larger splitting in DM2 can be suggested using this analogy. In our case, the incoupling is via near-field component of the incident photon: the time scale of the event equals the time the photon spends in the immediate vicinity of the surface. In other words, interpreting the dip in the reflection as destructive interference between the reflected light and SPP, the SPP excited by a photon can have propagated only of the order of the wavelength to interfere with the reflected component of the same incident photon (incoherent source). After this time, there is no possibility for the strongly coupled system to affect the signal measured by DM1. In this way, we enforce in DM1 a fast decay, i.e., a small effective interaction time. In contrast, for DM2, the interaction time of SPPs with the molecular film is only limited by the decay or scattering of SPPs; DM2 monitors also SPPs that have propagated of the order of the SPP coherence length. The longer path length in case of DM2 is like the larger number of round trips a photon makes in a higher *Q* cavity.

The above reasoning was tested by fabricating plasmonic silver waveguides where SPPs are launched at a certain location and, after propagating micrometers, go through an interaction area of R6G molecules in an SU-8 matrix on top of the waveguide. The emitted light at the end of the interaction area was collected by a 100× air objective (numerical aperture of 0.95) focused on the very end of the interaction area, and a spectrum was recorded by scanning the spectral region in 3 nm steps (for more details, see Refs. [10,11]). The launched SPPs have a broad spectrum peaked at 2.55 eV, overlapping with the studied R6G transitions. For the fabrication and measurements of such structures see our previous publications [10,11]. By limiting the length of the interaction area, we wanted to enforce a faster effective decay than given by the natural coherence times or lengths of the system, and thus effectively control the interaction time between R6G and SPP. One may

assume the SPP coherence length to be similar to the propagation length of SPP [26] (5 μm in our case [10]): we studied samples with the interaction area lengths of 1, 2, and 5 μm. As seen in Fig. 3, for the shortest area, only a broad peak around the R6G absorption and emission is visible (2.25 eV) [27]. The other peak (2.55 eV) is just due to the incoming noncoupled SPPs. For the 2 μm sample, a clear splitting is seen around the main absorption, and the peaks are narrowed from the 1 μm case. For 5 μm, also the second split at the absorption shoulder appears. Moreover, there is an additional feature possibly related to the R6G emission around 2.17 eV, indicating that also this transition is approaching the strong-coupling regime. It was carefully checked that the peaks are not due to Fabry-Perot—type resonances related to vertical or horizontal dimensions of the interaction area. Apart by the interaction area length, we increased the SPP-matter interaction by fabricating a layer of silver on top of the interaction area, thereby decreasing the mode volume and blocking the decay into radiative modes. With such a sample, the strong-coupling features become very prominent.

It should be noted that the high molecular concentration of our samples together with the tendency of R6G to form aggregates, particularly dimers [28,29], implies that dimers may contribute to the obtained dispersions and spectra. However, we believe that the main contribution to both splittings comes from monomers (see supplementary information for the discussion [30]).
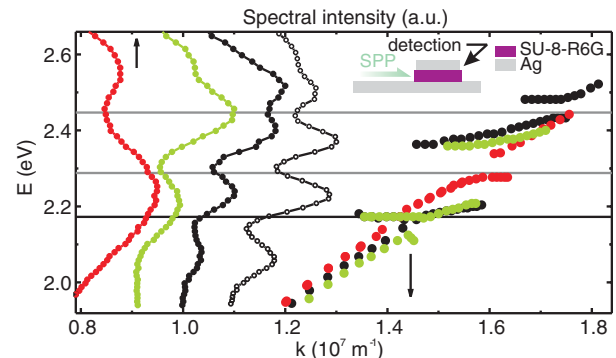

FIG. 3 (color online). The emission spectra measured from the waveguide samples having different lengths of R6G deposited on top of a waveguide (see the inset schematic), along with the dispersion curves of the thin film samples measured with DM2. The red, green, and black (or dark gray, gray, and black) spectra correspond to samples having 1, 2, and 5 μm lengths of R6G, respectively. The spectrum with empty black circles is measured from a waveguide sample having a 5 μm R6G area as well, but with a layer of silver deposited on top of this area (as in the schematic). In the dispersions red, green, and black (or dark gray, gray, and black) correspond to 4, 25, and 50 m*M* samples, respectively. The same color is used for pointing out the cases when the dips in the spectra and the splits in the dispersions appear at the same energies. The black horizontal line is the measured R6G emission and the gray lines absorption maximum and absorption shoulder energies.
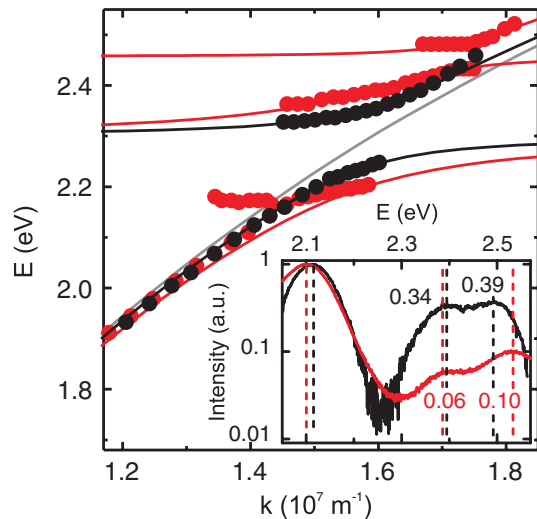
PHYSICAL REVIEW LETTERS

FIG. 4 (color online). The measured dispersions for 50 m*M* sample for DM1 (black) and DM2 (red or dark gray) and their theoretical fits. The solid gray curve is the theoretical dispersion of the uncoupled SPP on silver–SU-8 layer–air structure. The inset shows the normalized spectra for the 200 m*M* sample with DM1 (black) (background subtracted), and DM2 (red or dark gray), both with excitation light angle 71.5°. The dashed lines show the spectral peak positions for the measurement methods DM1 (black) and DM2 (red or dark gray). The numbers indicate the intensity of the peaks.

Finally, we consider the possible energy transfer between the hybrid modes [31,32]. The inset of Fig. 4 shows the normalized spectra of the 200 m*M* sample measured with both DM1 and DM2, with 71.5° incident angle. The relative intensity of the two high energy modes is lower for DM2. The highest energy mode has 1/4 and the middle one 1/6 intensity in DM2 as compared to DM1. The differences originate from the time evolution of the system: propagation speed, dissipation, and scattering properties of the modes, and/or energy transfer between the modes. Dissipation and scattering are nearly wavelength independent for the values considered [11], which indicates that energy transfer plays a considerable role. To confirm the existence of the energy transfer is, however, beyond the scope of this Letter.

In summary, we have demonstrated a double VRS for SPP and R6G molecules, despite the broad absorption of R6G. We therefore expect that the strong-coupling regime between SPPs and photoactive molecules is readily accessible for a wide variety of other molecules as well. For the first time, we demonstrate that each of the three energy branches of the strongly coupled SPP-molecule system can be converted into photons. Especially, *dynamics* was studied by comparison of the energies and intensities of the in- and outcoupled modes in reflectometry, and by a novel approach using waveguide experiments. In the latter case, the effective Rabi splitting was easily controlled by standard lithographical methods which is promising con-

sidering applications. The double split, as well as the potential of creating spatially separated interaction areas on the waveguides, opens up interesting possibilities for studies of multimode hybridization and energy transfer.

*paivi.torma@hut.fi
[1] C. Weisbuch *et al.*, Phys. Rev. Lett. **69**, 3314 (1992).
[2] G. Khitrova *et al.*, Nature Phys. **2**, 81 (2006).
[3] D. G. Lidzey *et al.*, Nature (London) **395**, 53 (1998).
[4] R. J. Holmes and S. Forrest, Org. Electron. **8**, 77 (2007).
[5] J. Bellessa *et al.*, Phys. Rev. Lett. **93**, 036404 (2004).
[6] J. Dintinger *et al.*, Phys. Rev. B **71**, 035424 (2005).
[7] I. Pockrand, A. Brillante, and D. Mobius, J. Chem. Phys. **77**, 6289 (1982).
[8] E. Kretschmann and H. Raether, Z. Naturforsch. **23A**, 2135 (1968).
[9] A. V. Zayats, I. I. Smolyaninov, and A. A. Maradudin, Phys. Rep. **408**, 131 (2005).
[10] A. Kuzyk *et al.*, Opt. Express **15**, 9908 (2007).
[11] T. K. Hakala *et al.*, Appl. Phys. Lett. **93**, 123307 (2008).
[12] M. S. Skolnick, T. A. Fisher, and D. M. Whittaker, Semicond. Sci. Technol. **13**, 645 (1998).
[13] D. G. Lidzey *et al.*, Science **288**, 1620 (2000).
[14] R. J. Holmes and S. R. Forrest, Phys. Rev. Lett. **93**, 186404 (2004).
[15] Y. Sugawara *et al.*, Phys. Rev. Lett. **97**, 266808 (2006).
[16] G. A. Wurtz *et al.*, Nano Lett. **7**, 1297 (2007).
[17] N. T. Fofang *et al.*, Nano Lett. **8**, 3481 (2008).
[18] P. A. Hobson *et al.*, Appl. Phys. Lett. **81**, 3519 (2002).
[19] G. Ritchie and E. Burstein, Phys. Rev. B **24**, 4843 (1981).
[20] M. A. Noginov *et al.*, Phys. Rev. Lett. **101**, 226806 (2008).
[21] C. Symonds *et al.*, Appl. Phys. Lett. **90**, 091107 (2007).
[22] C. Symonds *et al.*, New J. Phys. **10**, 065017 (2008).
[23] V. M. Agranovich, M. Litinskaia, and D. G. Lidzey, Phys. Rev. B **67**, 085311 (2003).
[24] J. P. Reithmaier *et al.*, Nature (London) **432**, 197 (2004).
[25] T. Yoshie *et al.*, Nature (London) **432**, 200 (2004).
[26] H. Ditlbacher *et al.*, Appl. Phys. Lett. **81**, 1762 (2002).
[27] The spectra in the Fig. 3 are shifted approximately 9 nm (40 meV) to compensate for instrument errors in the confocal microscopy. Even without this correction the spectra show high qualitative agreement with the measured dispersion curves.
[28] L. V. Levshin, M. G. Reva, and B. D. Ryzhikov, J. Appl. Spectrosc. **26**, 48 (1977).
[29] P. Bojarski, Chem. Phys. Lett. **278**, 225 (1997).
[30] See EPAPS Document No. E-PRLTAO-103-015933 for discussion of dimer contribution. For more information on EPAPS, see http://www.aip.org/pubservs/epaps.html.
[31] D. G. Lidzey *et al.*, J. Lumin. **110**, 347 (2004).
[32] J. Chovan *et al.*, Phys. Rev. B **78**, 045320 (2008).